

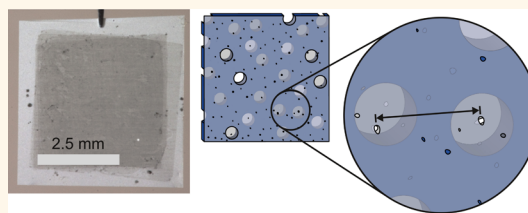
# Implications of Permeation through Intrinsic Defects in Graphene on the Design of Defect-Tolerant Membranes for Gas Separation

Michael S. H. Boutilier,<sup>†</sup> Chengzhen Sun,<sup>†,‡</sup> Sean C. O'Hern,<sup>†</sup> Harold Au,<sup>†</sup> Nicolas G. Hadjiconstantinou,<sup>†</sup> and Rohit Karnik<sup>†,\*</sup>

<sup>†</sup>Department of Mechanical Engineering, Massachusetts Institute of Technology, 77 Massachusetts Avenue, Cambridge, Massachusetts 02139, United States, and

<sup>‡</sup>State Key Laboratory of Multiphase Flow in Power Engineering, Xi'an Jiaotong University, Xianning West Road 28, Xi'an 710049, P.R. China

**ABSTRACT** Gas transport through intrinsic defects and tears is a critical yet poorly understood phenomenon in graphene membranes for gas separation. We report that independent stacking of graphene layers on a porous support exponentially decreases flow through defects. On the basis of experimental results, we develop a gas transport model that elucidates the separate contributions of tears and intrinsic defects on gas leakage through these membranes. The model shows that the pore size of the porous support and its permeance critically affect the separation behavior, and reveals the parameter space where gas separation can be achieved regardless of the presence of nonselective defects, even for single-layer membranes. The results provide a framework for understanding gas transport in graphene membranes and guide the design of practical, selectively permeable graphene membranes for gas separation.



**KEYWORDS:** graphene membranes · gas separation · multilayer graphene · nanofiltration · nanofluidics

Separating the components of a gaseous mixture is a critical step in several important industrial processes including natural gas purification, hydrogen production, carbon dioxide sequestration, and oxy-combustion.<sup>1–4</sup> Membrane separation systems offer definite benefits compared to conventional cryogenic and sorption-based methods, especially for small-to-medium scale applications.<sup>1</sup> Membrane separations employ no moving parts, require no exotic chemicals, and typically exhibit low energy requirements and flexibility in configuration.<sup>4</sup> However, the inherent trade-off between the permeability and selectivity of conventional membrane materials has largely limited gas separation membranes to systems requiring relatively low production rates or to mixtures with high impurity concentrations in the feed gas.<sup>5</sup>

In contrast, graphene gas separation membranes have the potential to significantly surpass the permeance and selectivity limits of conventional membranes.<sup>6,7</sup> With this single atom thick material, it is

possible to create subnanometer-scale pores that allow smaller gas molecules to pass through but produce a physical barrier severely limiting the passage of larger molecules.<sup>8</sup> Theoretical studies employing various computational and analytical tools have predicted permeance and selectivity values for various graphene pore geometries that are orders of magnitude higher than have been achieved with existing membrane technology.<sup>6,7,9–11</sup> The feasibility of constructing such selective pores was recently demonstrated by Koenig *et al.*<sup>8</sup> using micrometer-scale graphene membranes in which pores were created by UV-induced oxidative etching. They were able to produce two graphene membranes with selectivities of approximately 15 000, one being strongly permeable to gas molecules with kinetic diameters smaller than 3.4 Å and the other permeable to gases with kinetic diameters smaller than 4.9 Å.

However, the imperfect quality of large areas of graphene presents a significant challenge in scaling such single-layer graphene

\* Address correspondence to karnik@mit.edu.

Received for review October 23, 2013 and accepted December 20, 2013.

Published online January 03, 2014  
10.1021/nn405537u

© 2014 American Chemical Society

membranes to macroscopic sizes. Small areas of pristine graphene are impermeable even to helium,<sup>12</sup> but due to the difficulty in isolating large areas of pristine graphene, macroscopic graphene membranes inherently have a nonzero permeance due to the presence of defects in the graphene.<sup>13</sup> These defects include intrinsic nanometer-scale holes that develop during the graphene growth process, and tears or other micrometer-scale gaps in the graphene that form during the membrane manufacturing process.<sup>13</sup> Gas leakage through micrometer-scale tears and nanometer-scale intrinsic defects in macroscopic graphene membranes can severely limit their selectivity and make separation impossible. Indeed, to date gas separation has been demonstrated only in multilayered membranes prepared from graphene oxide,<sup>14–16</sup> where permeance is 3–4 orders of magnitude lower than that predicted by simulations across single-layer graphene membranes. Even in these multilayer membranes, gas transport through defects can play a role in addition to interlayer transport.<sup>15</sup> It is therefore critical to understand transport through intrinsic defects and tears in graphene and to develop strategies to mitigate nonselective leakage if the full potential of graphene membranes for gas separation is to be realized.

In this paper, we quantify the effects of tears and intrinsic defects on the gas permeance and separation performance of graphene composite membranes (GCM) comprising graphene situated on a porous support membrane. We show that independent stacking of two to five layers of graphene is a promising method for reducing the effects of defects while maintaining the nanometer-scale thickness of the graphene layer. The inherent permeance of these multilayer macroscopic graphene membranes is measured and a gas transport model is developed that can accurately explain the experimentally observed flow rates. From this model, the separate contributions of tears and intrinsic defects to the inherent permeance of macroscopic graphene membranes are estimated. This model is further used to identify design constraints for realizing selectively permeable graphene membranes for gas separation.

## RESULTS AND DISCUSSION

**Graphene Composite Membranes.** Graphene composite membranes were fabricated by transferring graphene grown on copper foil by chemical vapor deposition (CVD) to a polycarbonate track-etched membrane (PCTEM) support using a direct transfer method developed previously (Figure 1a).<sup>13</sup> PCTEMs were chosen as the porous support because they contain a high density of straight, well-defined pores with uniform sizes<sup>17</sup> that can be tuned from 10 nm to over 10  $\mu\text{m}$ . The porous support allows the graphene layer to be handled without damage.<sup>13</sup> The series of parallel pore

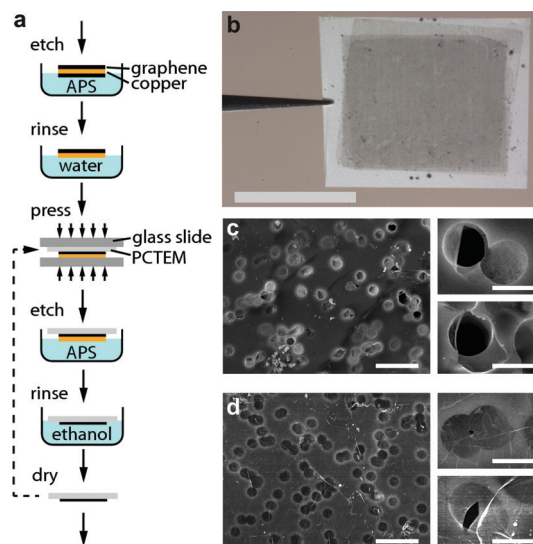


**Figure 1.** Graphene composite membranes. (a) Membrane fabrication process by direct transfer of graphene from copper foil to a polycarbonate track-etched membrane (PCTEM). The copper foil was etched using ammonium persulfate (APS). Multilayer graphene composite membranes were fabricated by repeated application of the one layer transfer process. (b) Photograph of a four-layer graphene composite membrane. Scale bar, 5 mm. (c and d) SEM images of a (c) one-layer and (d) five-layer graphene membrane and tears. Scale bars are 5 and 1  $\mu\text{m}$ .

channels in the PCTEM also isolate small areas of graphene, such that the graphene composite membrane is effectively formed from numerous smaller graphene membranes arrayed in parallel. Flow through any defect in the graphene is restricted by the narrow channels in the PCTEM, which can potentially prevent leakage from dominating over the flow through intentionally created selective pores.

In addition, we hypothesized that the effects of leakage may be further mitigated by independently stacking multiple layers of graphene on the porous support, so that defects in one layer are covered by another layer. To achieve this goal, the transfer process was repeated to create GCMs with multiple independently stacked layers of graphene (Figure 1a). In a multilayer graphene composite membrane (Figure 1b), individual layers of graphene can be distinguished by the successively darker areas over the white PCTEM. Scanning electron microscope (SEM) images of GCMs with a single layer of graphene (Figure 1c) clearly show several polycarbonate pores with micrometer-scale tears in their graphene coverage. In contrast, SEM images of a five layer graphene membrane (Figure 1d) show a much smaller fraction of tears as compared to the single layer membrane. The images clearly show that independently stacked graphene layers improve graphene coverage on the PCTEM.

**Independent Stacking of Multiple Layers of Graphene Reduces Leakage.** Gas transport through the GCMs was measured by supplying the desired gas on the graphene side of the membrane and monitoring the

pressure rise in a downstream reservoir (Figure 2a, inset). Transferring a single layer of graphene onto a PCTEM reduced the flow rate of helium through the PCTEM by approximately 60%, as seen in Figure 2a. Since no selective pores were created in graphene, we expect that the residual 40% leakage represents helium flow through intrinsic defects and tears in the graphene. Next, we examined helium flow rates through GCMs with one to five layers of graphene, and observed an exponential reduction in the helium flow rate as the number of graphene layers was increased (Figure 2). By stacking multiple layers of graphene on a PCTEM, it was possible to produce a macroscopic graphene membrane with a 99% smaller permeance (*i.e.*, only 1% leakage) compared to the bare support membrane. Furthermore, the apparent exponential decay of helium flow rates with increasing number of layers of graphene suggests that approximately the same fraction of polycarbonate pores are covered by graphene in each layer, and that the locations of the micrometer-scale tears in each layer are independent of those in the other layers.

**Modeling Transport through Graphene Composite Membranes.** We developed a model to quantitatively understand the effects of defects and independent stacking of graphene layers on the gas transport behavior of the membranes. Since pristine graphene is impermeable

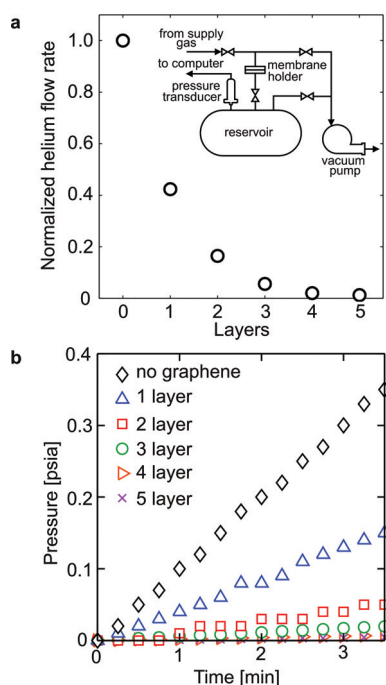


**Figure 2.** Measurements of gas flow rates through graphene composite membranes with multiple layers of graphene. (a) Effect of the number of layers of graphene on helium flow rate, normalized by the flow rate through a bare PCTEM. Data points represent flow rates measured through different GCMs that were manufactured in parallel. Inset shows a sketch of the gas flow measurement setup. (b) Time traces of pressure rise in the downstream reservoir during helium flow rate measurements for the membranes.

to gases,<sup>12</sup> we assume that the net permeance is a result of flow through micrometer-scale tears over the PCTEM pores (see Figure 1c,d), intrinsic nanometer-scale defects dispersed across areas of continuous graphene,<sup>13</sup> and any intentionally created selective nanopores (Figure 3).

We account for any micrometer-scale tears by assuming that each layer of graphene covers a fraction  $\gamma$  of the pores in the PCTEM support, with subsequent layers covering the same fraction of pores independent of the other layers (Figure 3a,b). As a result, a two-layer graphene membrane has polycarbonate pores with zero, one, or two layers of graphene (Figure 3c). For a general  $N$ -layer graphene composite membrane, the fraction of polycarbonate pores with  $n$  layers of graphene coverage,  $\gamma_n$ , is given by,

$$\gamma_n = \frac{N!}{n!(N-n)!} (1-\gamma)^N - n\gamma^n \quad (1)$$

When multiple layers of graphene are stacked, we assume that intrinsic defects in one layer are covered by graphene in another layer, except where intrinsic

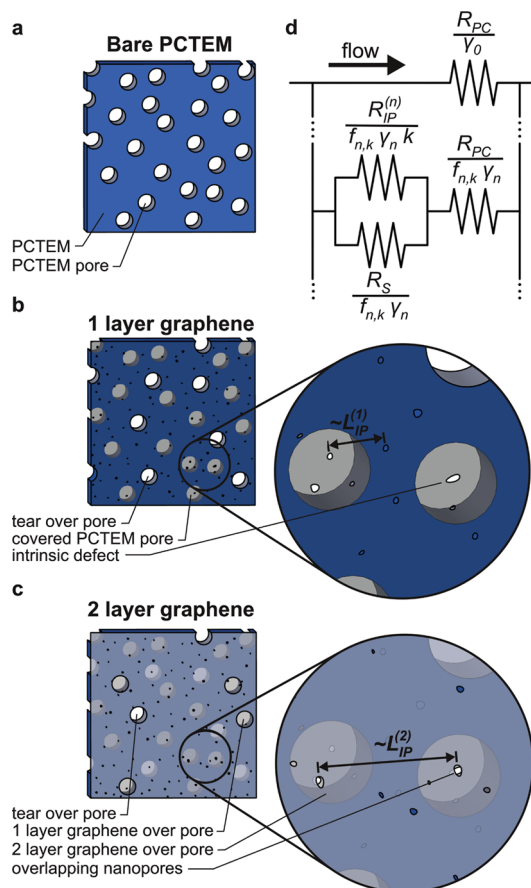


**Figure 3.** Transport pathways considered in the gas flow rate model. (a–c) Illustration of the change in tears and intrinsic defects over polycarbonate track-etched pores upon transferring (b) one and (c) two layers of graphene onto the PCTEM. (d) Equivalent resistance network for flow through GCMs. Note that  $R_{PC} = 4(\pi D_{PC}^2 P_{PC}^A)^{-1}$ ,  $R_S = 4(\pi D_{PC}^2 P_S^A)^{-1}$ , and  $R_{IP}^{(n)} = (L_{IP}^2 P_{IP,n}^A)^{-1}$ .

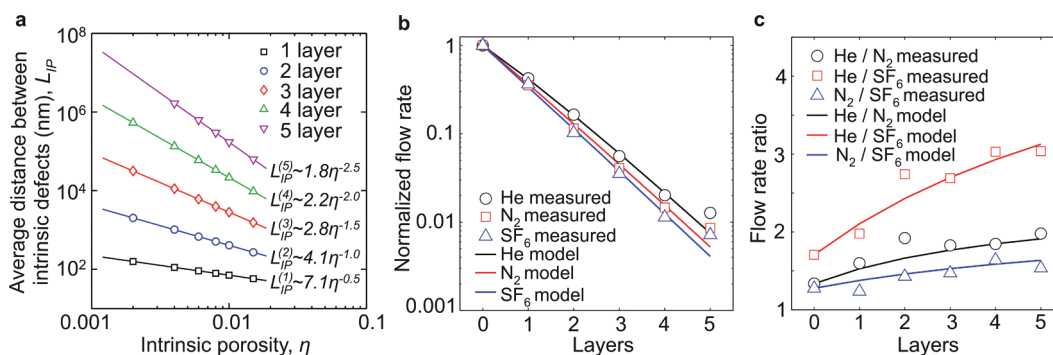


**Figure 4.** Multiple layer graphene composite membrane flow rate measurements and model fit. (a) Computed average distance between intrinsic defects in multilayer graphene membranes. (b) Flow rate model fit, giving a coverage of 69.8% ( $\gamma = 0.698$ ) and an intrinsic porosity of 0.687% ( $\eta = 0.00687$ ). Flow rates are normalized by the value for a bare PCTEM. (c) Measured flow rate ratios compared to model fit for flow rates.

defects in all layers randomly align. The average distance between intrinsic defects in one-layer graphene,  $L_{IP}^{(1)}$ , was obtained from the defect size distribution data in ref 13 (where we reported characterization of graphene from the same source), combined with the intrinsic porosity of graphene,  $\eta$ , *i.e.*, the fraction of graphene area occupied by intrinsic defects. The average spacing between aligned intrinsic defects in  $n$  stacked layers of graphene,  $L_{IP}^{(n)}$ , was computed by Monte Carlo simulations (see Supporting Information Section 1 for details). Given the spacing between aligned intrinsic defects, the fraction of polycarbonate pores (of diameter  $D_{PC}$ ) with  $n$  layers of graphene that have  $k$  aligned intrinsic defects can then be calculated from the Poisson distribution,

$$f_{n,k} = \frac{1}{k!} \left[ \frac{\pi}{4} \left( \frac{D_{PC}}{L_{IP}^{(n)}} \right)^2 \right]^k \exp \left[ -\frac{\pi}{4} \left( \frac{D_{PC}}{L_{IP}^{(n)}} \right)^2 \right] \quad (2)$$

To limit complexity, we assumed identical permeance for all intrinsic defects regardless of the size, an assumption that was independently validated (see Supporting Information Section 1.3). The average permeance due to intrinsic defects in  $n$ -layer graphene ( $P_{IP,n}^A$ ) was estimated as the equilibrium ideal gas flux through the fraction of graphene area occupied by aligned intrinsic defects, assuming that the intrinsic pores are much larger than the gas molecules. Finally, any selective nanopores intentionally introduced into the graphene will provide a flow path in parallel to the intrinsic defects. We assume that their density is sufficiently high to represent flow through these nanopores by an average selective pore permeance,  $P_S^A$ , defined as the molar flow rate per unit graphene area per unit pressure difference.

Gas transport through the graphene membrane was computed using an equivalent resistance network<sup>18</sup> (Figure 3d). Each branch of this network represents polycarbonate pores with a certain number of layers of graphene coverage and a certain number of intrinsic defects. The graphene composite

membrane permeance for arbitrary gas  $A$  is then computed as,

$$P^A = \gamma_0 P_{PC}^A + \sum_{n=1}^N \sum_{k=0}^{\infty} \gamma_n f_{n,k} \left[ \frac{1}{P_{PC}^A} + \left( \frac{4k}{\pi} P_{IP,n}^A \left( \frac{L_{IP}^{(n)}}{D_{PC}} \right)^2 + P_S^A \right)^{-1} \right]^{-1} \quad (3)$$

The polycarbonate permeance ( $P_{PC}^A$ ) for each gas was measured on a bare PCTEM without any graphene (see Supporting Information Section 2 and Figure S9). This leaves three unspecified parameters for this model: (1) the fraction of polycarbonate pores covered by a single layer of graphene,  $\gamma$ , (2) the fraction of graphene area occupied by intrinsic defects,  $\eta$ , and if applicable, (3) the intentionally created selective nanopore permeance,  $P_S^A$ .

**Model Predicts Transport Characteristics of Independently Stacked Graphene Membranes.** The number density and distance between intrinsic defects is an important parameter governing the membrane performance. Power-law fits to the Monte Carlo simulation results for a range of intrinsic porosities (Figure 4a) show a scaling  $(L_{IP}^{(n)})^{-2} \sim \eta^n$ , *i.e.*, the average number density of aligned intrinsic defects in independently stacked layers of graphene decreases as the  $n$ th power of the intrinsic porosity of graphene. This scaling behavior is explained by the fact that when a layer of graphene with porosity  $\eta$  is placed on a previous layer, only a fraction  $\eta$  of the existing defects align with defects in the new layer. Therefore, each successive layer reduces the number of defects by a fraction  $\eta$ . The exact coefficients of the scaling relations depend on the intrinsic defect size distribution.

Next, we compared model predictions (Supporting Information Section 1.3) of gas transport through the multilayer membranes with measured flow rates of gases with a range of molecule sizes (He, N<sub>2</sub>, and SF<sub>6</sub>, with kinetic diameters of 2.6, 3.64, and 5.5 Å, respectively<sup>19</sup>), without any intentionally created selective nanopores ( $P_S^A = 0$ , Figure 4b,c). With least-squares fitting, the graphene composite

membrane characteristics were well described by  $\gamma = 0.698$  and  $\eta = 6.87 \times 10^{-3}$ . The model results accurately matched the exponential decrease of measured flow rates as the number of layers of graphene was increased from one to four (Figure 4b). The model also captures the gradual rise in flow rate ratios of the gases with increasing number of graphene layers. Since the intrinsic defects were measured to be larger than the kinetic diameter of the gases, the intrinsic defect selectivity is approximately  $P_{P,1}^A/P_{P,1}^B = (M_B/M_A)^{1/2}$  from the kinetic theory of gases, which is somewhat higher than that for flow through the polycarbonate pores (Figure S10b). As a result, increasing the contribution of intrinsic defects compared to tears upon adding more layers of graphene causes a slight increase in the flow rate ratio.

Quantitative agreement between the experimentally measured and theoretical flow rate and flow rate ratio with increasing number of graphene layers provides validation for the model developed here. The model was further verified by comparing its predictions to those of a more detailed model, discussed in Supporting Information Section 1. We considered the possibility that the deviation of the model trends from the measured flow rates for five layer graphene composite membranes (Figure 4b) is in-plane gas transport between layers of graphene, which scales weakly (inversely) with the number of layers and will eventually govern transport as the number of layers increases. If the deviation for the five-layer membrane is attributed entirely to in-plane transport, we can estimate a conservative lower bound on in-plane transport resistance of  $1.2 \times 10^4 \text{ Pa} \cdot \text{s} \cdot \text{m}^2/\text{mol}$  for helium, corresponding to an interlayer diffusivity of  $1.2 \times 10^{-15} \text{ m}^3/\text{s}$  (see Supporting Information Section 3). However, such a low interlayer transport resistance would cause significant deviation between measured flow rates and model predictions for two, three, and four layer membranes, which we do not observe. Therefore, it is concluded that interlayer transport is not responsible for the deviation between model and measured flow rates for the five layer membranes in Figure 4b, and the computed in-plane transport resistance represents a very conservative lower bound. The discrepancy between the measurements and model predictions for the five layer membrane in Figure 4b is thus likely due to damage induced during the repeated mechanical pressing steps, which could become a significant factor at low flow rates.

A recent report in which transport across stacked graphene layers was measured speculated that the increase in flow rate ratio is due to interlayer transport.<sup>15</sup> Our experiments and modeling results indicate that the permeability for interlayer transport in graphene is low and that intrinsic defects alone can account for the increased selectivity observed from stacking successive layers. This result is consistent with measurements of in-plane gas diffusion along a

graphene–copper interface, which show significantly lower transport than has been observed between layers of graphene oxide.<sup>20</sup>

**Feasibility of Selective Transport in the Presence of Non-selective Defects.** We now use the gas transport model to explore whether gas separation may be accomplished in macroscopic, single- or few-layer graphene membranes regardless of the presence of defects for two model gases, He and SF<sub>6</sub>. To do this, we estimated intentionally created selective nanopore permeances, and used these in the model to predict overall membrane selectivities in the presence of intentionally created selective nanopores. On the basis of molecular dynamics simulations<sup>9</sup> and gas flux measurements by Koenig *et al.*<sup>8</sup> (assuming that the reported flux corresponds to one measured pore), the achievable resistance of a single selective nanopore to He is estimated to be in the range of  $9 \times 10^{19}$  to  $2 \times 10^{22} \text{ Pa} \cdot \text{s}/\text{mol}$ . We further assume a selective pore density of  $10^{12} \text{ cm}^{-2}$  (one nanopore per  $10 \times 10 \text{ nm}^2$  area) to calculate the permeance due to selective pores,  $P_S^{\text{He}}$ . On the basis of the measurements of Koenig *et al.*,<sup>8</sup> the selective pore selectivity is set to  $P_S^{\text{He}}/P_S^{\text{SF}_6} = 15\,000$ .

The available graphene quality (specified by  $\eta = 6.87 \times 10^{-3}$  and  $L_p^{(n)}$  in Figure 4a) and the graphene permeance due to selective pores are limited by the graphene synthesis and selective pore creation procedures. However, it is possible to precisely control the support membrane pore size and permeance, and to enhance the graphene coverage through the graphene transfer process and the number of layers used. The model predicts that for the  $1 \mu\text{m}$  diameter polycarbonate membranes with  $\sim 70\%$  graphene coverage fabricated in this study, it is unlikely that any selectivity will be obtained even with five layers of graphene for the expected range of selective pore permeance (Figure 5, top left plot). This lack of selectivity results primarily from the high permeance of polycarbonate pores, causing leakage through micrometer-scale tears to dominate. By increasing the polycarbonate pore resistance to mitigate the effect of leaks through tears, it is possible to achieve modest selectivity with five layers of graphene (top row of plots in Figure 5). Further increase in polycarbonate pore resistance reduces selectivity because flow is then limited by the nonselective polycarbonate pores.

Using polycarbonate membranes with the smallest commercially available pore size of 10 nm shows the potential for much better selectivity, using the experimentally measured resistance of those polycarbonate membranes (center row of plots in Figure 5). Since the support membrane pore diameter is much smaller than the average distance between intrinsic defects (see Figure 4a), it tends to isolate the defects to only a small fraction of graphene-covered polycarbonate pores, leaving the majority of the pores covered with defect-free graphene. Three layers of graphene and

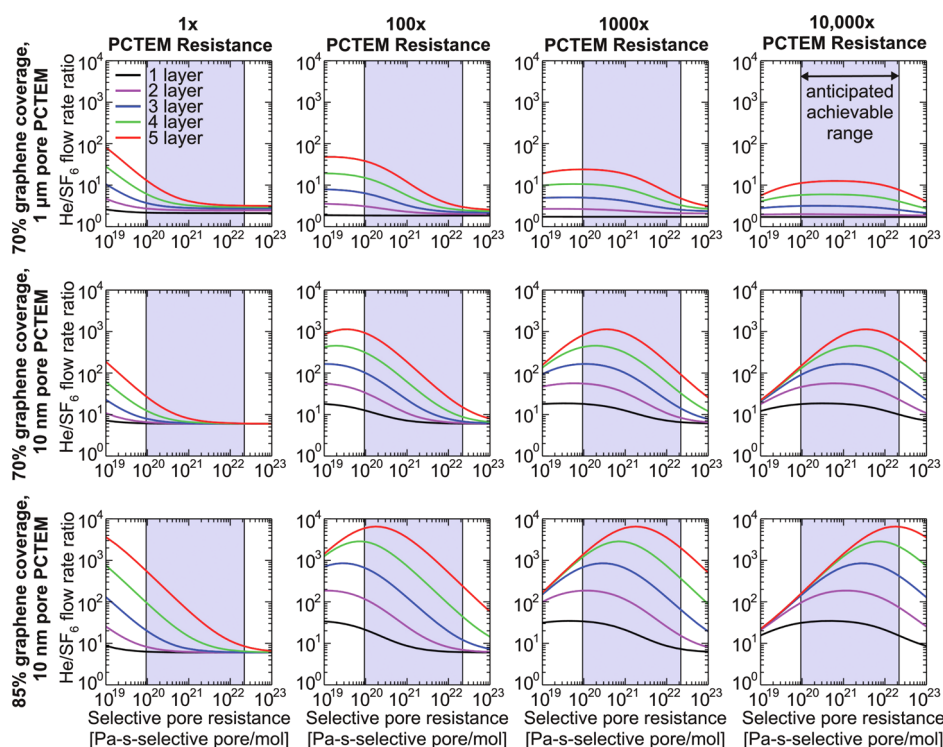


**Figure 5.** Model predictions of helium (He) to sulfur hexafluoride (SF<sub>6</sub>) flow rate ratios for various values of graphene fractional area coverage ( $\gamma$ ), support membrane pore diameter ( $D_{PC}$ ), and support membrane pore resistance ( $R_{PC}$ ).

a factor of 1000 increase of the polycarbonate pore resistance further mitigates leaks, yielding selectivities on the order of 100. With a modest increase in the fractional area coverage of graphene from 70% to 85%, selectivities on the order of 1000 are feasible (bottom row of plots in Figure 5). These results suggest the feasibility of gas separation using graphene with typical quality obtained by chemical vapor deposition, provided that an appropriate porous support is chosen.

**Dimensionless Parameters Defining Regimes of Selective Transport.** We now specify dimensionless parameters to define gas permeation regimes through graphene membranes for the purpose of guiding their design and optimization. For simplicity, we focus on membranes with a single layer of graphene and omit notations specifying the number of layers. Given two gases  $A$  and  $B$ , under the assumptions that intrinsic defects are nonselective and that the polycarbonate pore resistances for both gases are equal to those under rarefied gas flow, we can express the membrane selectivity  $P^A/P^B$  in terms of dimensionless parameters as follows (see Supporting Information Section 1.3):

$$\frac{P^A}{P^B} = f\left(\gamma, \frac{L_{IP}}{D_{PC}}, \frac{P_{PC}}{P_S^A}, \frac{P_{IP}}{P_S^A}, \frac{P_S^B}{P_S^A}\right) \quad (4)$$

The number of intrinsic defects per polycarbonate pore is proportional to  $(D_{PC}/L_{IP})^2$ .  $P_{PC}/P_S^A$  and  $P_{IP}/P_S^A$  define the permeance of the support membrane and intrinsic defects, respectively, relative to that due to selective pores, while the selectivity of the selective

pores is defined by  $P_S^A/P_S^B$  (assumed equal to 15 000 here, see Supporting Information Section 1).

Analytical expressions for the GCM selectivity ( $P^A/P^B$ ) function in eq 4 and corresponding GCM permeance ( $P^A/P_S^A$ ) are derived in Supporting Information Section 1.3. Given a certain intrinsic defect permeance ( $P_{IP}/P_S^A$ ), both the GCM selectivity ( $P^A/P^B$ ) and permeance ( $P^A/P_S^A$ ) are defined by the choice of support permeance ( $P_{PC}/P_S^A$ ) and intrinsic defect spacing relative to the support pore size ( $L_{IP}/D_{PC}$ ). This results in a trade-off between the selectivity ( $P^A/P^B$ ) and permeance ( $P^A/P_S^A$ ), illustrated for  $P_{IP}/P_S^A = 0.01$  and  $P_{IP}/P_S^A = 1$  for  $\gamma = 0.99$  (Figure 6a,b). When the permeance of intrinsic defects is small (Figure 6a), high GCM selectivity can be achieved for any value of  $L_{IP}/D_{PC}$ . However, for  $P_{IP}/P_S^A = 1$  (Figure 6b), high selectivity is only achieved when the spacing between intrinsic defects is large compared to the support pore diameter ( $L_{IP}/D_{PC} \gtrsim 1$ ). This illustrates that, when the selective pore permeance dominates over the intrinsic defect permeance, intrinsic defects in the graphene over the support membrane pore will not compromise selectivity. However, when the intrinsic defect permeance is significant, it is important that the support membrane pore diameter be sufficiently smaller than the intrinsic defect spacing, so that the intrinsic defects will be isolated to a small fraction of the support pores, leaving a large number of support pores with high selectivity. In addition to the dependence on  $L_{IP}/D_{PC}$ , the membrane is selective only for a certain range of permeance

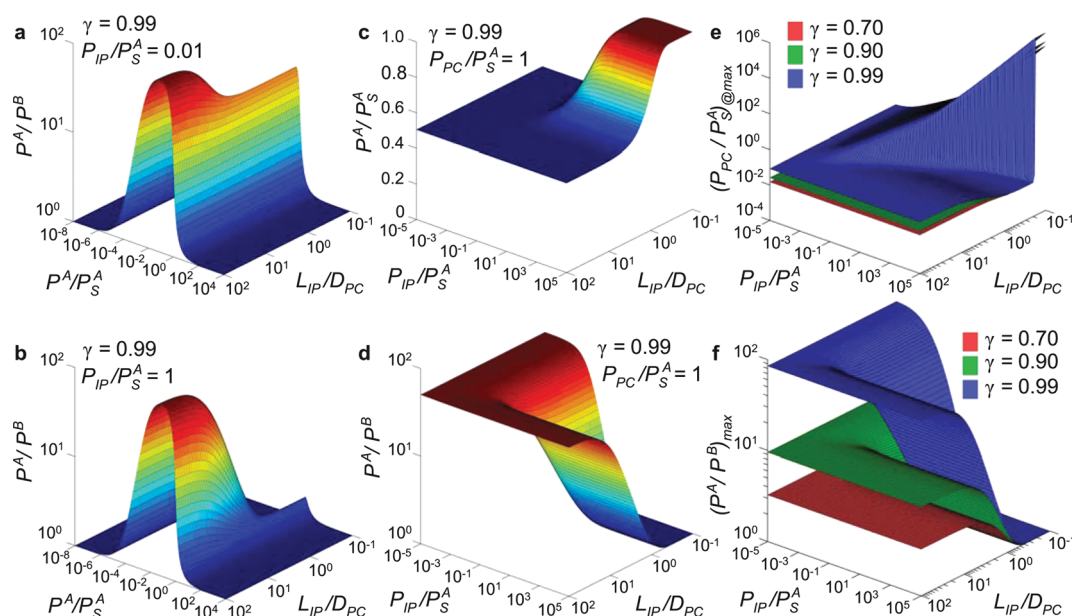


**Figure 6.** Model predictions of the general GCM permeance characteristics. (a and b) Dependence of GCM selectivity ( $P^A/P^B$ ) on GCM permeance ( $P^A/P_S^A$ ) and intrinsic defect spacing ( $L_{IP}/D_{PC}$ ) for 99% coverage ( $\gamma = 0.99$ ) and intrinsic defect permeance of (a)  $P_{IP}/P_S^A = 0.01$  and (b)  $P_{IP}/P_S^A = 1$ . (c and d) Dependence of (c) GCM permeance ( $P^A/P_S^A$ ) and (b) GCM selectivity ( $P^A/P^B$ ) on the intrinsic defect permeance ( $P_{IP}/P_S^A$ ) and intrinsic defect spacing ( $L_{IP}/D_{PC}$ ) for 99% coverage ( $\gamma = 0.99$ ) when the support membrane is matched to that of the selective pores ( $P_{PC}/P_S^A = 1$ ). (e) Support membrane permeance ( $P_{PC}/P_S^A$ ) that maximizes GCM selectivity ( $P^A/P^B$ ) for various graphene area coverage fractions ( $\gamma$ ), intrinsic defect permeances ( $P_{IP}/P_S^A$ ), and intrinsic defect spacings ( $L_{IP}/D_{PC}$ ), and (f) corresponding maximum GCM selectivities ( $P^A/P^B$ ).

$P^A/P_S^A$ . Nonselective transport through tears result in poor selectivity at high  $P^A/P_S^A$ , corresponding to high  $P_{PC}/P_S^A$ , whereas the dominant nonselective backing membrane resistance prevents selective transport at low  $P^A/P_S^A$ , corresponding to low  $P_{PC}/P_S^A$ . Selectivity is observed at intermediate  $P^A/P_S^A$  values, when the support resistance approaches the selective pore permeance  $P_{PC}/P_S^A \sim 1$ . Further decrease in the support permeance decreases the total permeance by several orders of magnitude for only modest gain in selectivity.

When the support membrane resistance matches that of the selective pores ( $P_{PC}/P_S^A = 1$ ), high permeance occurs for large  $P_{IP}/P_S^A$  and small  $L_{IP}/D_{PC}$  (Figure 6c), for which all support pores have highly permeable intrinsic defects in the graphene over them resulting in poor selectivity (Figure 6d). Under these conditions,  $P^A/P_S^A = P_{PC}/P_S^A = 1$ , because the resistance of the graphene becomes negligible compared to that of the support membrane. For low intrinsic defect permeance  $P_{IP}/P_S^A$  or large spacing between intrinsic defects  $L_{IP}/D_{PC}$ , transport through intrinsic defects becomes negligible and the permeance approaches  $P^A/P_S^A = (1 - \gamma)P_{PC}/P_S^A + \gamma/(1 + P_S^A/P_{PC})$ , as shown in Supporting Information Section 1.4. It is immediately seen from Figure 6d that, even for a properly balanced membrane where the support membrane resistance matches that of the selective pores, selective transport is possible only if either of the two criteria are met: (a) the permeance due to intrinsic defects is small compared to the permeance due to selective pores ( $P_{IP}/P_S^A \lesssim 1$ ), OR (b) the spacing between intrinsic defects is large

compared to the support pore diameter ( $L_{IP}/D_{PC} \gtrsim 1$ ). The first criterion implies insignificant leakage through intrinsic defects. We find that this is practically unlikely for the currently available quality of graphene, based on the estimated  $\eta$  and permeance due to selective pores, which suggest  $2 \lesssim P_{IP}/P_S^A \lesssim 2 \times 10^4$ . However, if leakage due to intrinsic defects is negligible with advances in graphene quality and selective pore creation, the selectivity is governed by micrometer-scale tears. For  $P_{PC}/P_S^A = 1$ , the selectivity approaches  $P^A/P^B = [1 - (1/2)\gamma]/(1 - \gamma)$  for infinite selectivity ( $P_S^A/P_S^B \rightarrow \infty$ ), and is only slightly lower for  $P_S^A/P_S^B = 15\,000$  (Supporting Information Section 1.4). The second criterion results in isolation of intrinsic defects. Under these conditions, most of the support membrane pores have no intrinsic defects in the graphene suspended over them and flow through intrinsic defects can be restricted by controlling the support membrane pore resistance, enabling high overall membrane selectivity. Leakage is then limited to the remaining pores that have graphene with intrinsic defects, approaching the same selectivity limit,  $P^A/P^B = [1 - (1/2)\gamma]/(1 - \gamma)$ . The nonselective regime occurs when these two criteria are not satisfied, and it is not possible to achieve selectivity through control of the support membrane resistance. In this regime, the support membrane pore diameter is larger than the average distance between intrinsic defects ( $L_{IP}/D_{PC} < 1$ ), resulting in most of the support membrane pores having intrinsic defects in the graphene over them. Consequently, the gas flow into the support membrane pores is dominated by the

lower resistance path through the intrinsic defects, bypassing the selective nanopores and producing no detectable overall membrane selectivity.

We now address the question of how to select an appropriate support membrane to achieve gas separation for graphene of a given quality, as characterized by the distance between intrinsic defects and the permeance due to intrinsic defects. The support membrane permeance that maximizes selectivity and the corresponding maximum possible selectivity depend on the quality of graphene (Figure 6e,f). As in Figure 6d, selectivity requires either low  $P_{IP}/P_S^A$  or high  $L_{IP}/D_{PC}$ . Under these conditions, the GCM approaches a limiting selectivity of  $P^A/P^B = 1/(1 - \gamma)$  for  $P_S^A/P_S^B \rightarrow \infty$  rather than the selectivity of  $P^A/P^B = [1 - (1/2)\gamma]/(1 - \gamma)$  obtained for the nonoptimal value of  $P_{PC}/P_S^A = 1$  shown in Figure 6d. For finite  $P_S^A/P_S^B$ , the GCM selectivity is maximized at low  $P_{IP}/P_S^A$  or high  $L_{IP}/D_{PC}$  to  $P^A/P^B = \{[(P_S^B/P_S^A)(1 - \gamma)]^{1/2} + 1\} / \{(P_S^B/P_S^A)^{1/2} + (1 - \gamma)^{1/2}\}$  (Figure 6f, Supporting Information Section 1.4) with a support membrane permeance of  $P_{PC}/P_S^A = [(P_S^B/P_S^A)/(1 - \gamma)]^{1/2}$  (Figure 6e). However, as seen by comparing the plot in Figure 6f to Figure 6d for  $\gamma = 0.99$ , selectivity is not significantly compromised with a membrane permeance of  $P_{PC}/P_S^A = 1$  instead of the optimal value of  $P_{PC}/P_S^A = 0.082$ , due to the relatively wide peak observed for high  $L_{IP}/D_{PC}$  in Figure 6a,b. However, choosing a support permeance  $P_{PC}/P_S^A = 0.082$  drastically compromises the overall membrane permeance, which shows that approximately matching the support permeance to that of selective pores ( $P_{PC}/P_S^A \sim 1$ ) may be preferable to choosing a support permeance that optimizes selectivity.

These results demonstrate that by choosing a support membrane with appropriate resistance and with a smaller pore size than the average distance between intrinsic defects, it is possible to achieve selective gas transport despite the presence of defects. While we have discussed the design of a porous support with isolated cylindrical pores, the results can also inform the design of membranes where the support comprises a thin isotropic layer with controlled permeance. In this case, the thickness of the layer is the

characteristic dimension that replaces the support pore diameter  $D_{PC}$  in the above analysis, *i.e.*, it is important to choose a thickness that is smaller than the spacing between intrinsic defects. The results in Figure 6 can then be used to identify the appropriate support membrane pore size (or thickness) and permeance once the graphene coverage, intrinsic defect characteristics, and achievable selective pore performance have been estimated.

## CONCLUSIONS

Realizing the full potential of graphene for use in gas separation membranes on a macroscopic scale will require understanding and controlling the adverse effects of micrometer-scale tears and nanometer-scale intrinsic defects in the graphene. We quantified these effects by measuring the permeance of macroscopic graphene composite membranes to different gases. It was shown that, by stacking individual layers of graphene, it is possible to exponentially reduce leakage through defects in the membrane. A model for gas permeance through macroscopic graphene membranes accounting for micrometer-scale tears and nanometer-scale intrinsic defects was developed and shown to accurately explain measured flow rates. The contributions of tears and intrinsic defects to the overall permeance of the membrane were quantified by fitting this model to the measured permeance values. The results indicate that interlayer transport is negligible in graphene membranes, and intrinsic defects can give rise to a modest selectivity. The graphene permeance model was applied to estimate selectivities of graphene composite membranes with intentionally created selective nanopores. Although tears and intrinsic defects have a detrimental effect on the overall membrane selectivity, the model shows that by controlling support membrane pore size and resistance, it is possible to design a selectively permeable graphene composite membrane. Model predictions of the optimal support membrane specifications are provided for a wide range of graphene characteristics to guide in the design of defect-tolerant selectively permeable graphene composite membranes for gas separation.

## METHODS

**Membrane Fabrication.** Multiple layers of graphene were stacked on a polycarbonate track-etched membrane (PCTEM) support by repeated application of the process for transferring a single layer of graphene onto PCTEMs developed in ref 13. This procedure is outlined in Figure 1a. Graphene on copper foil (ACS Materials) grown by chemical vapor deposition (CVD) was first cut into approximately 5 mm squares and the back sides of these pieces were etched for 5 min in ammonium persulfate (APS-100, Transene) to expose the copper and reduce the foil thickness. After a rinsing step, the piece of graphene on copper foil was mechanically pressed onto a larger PCTEM with 1  $\mu\text{m}$  pores and without a polyvinylpyrrolidone coating (Sterlitech).

The remaining copper foil was then completely removed by floating the stack on an ammonium persulfate solution. The resulting composite membrane, composed of a single layer graphene on a PCTEM, was then rinsed in ethanol before air drying. Subsequent layers of graphene were transferred one-by-one by mechanically pressing graphene on copper foil onto a PCTEM onto which graphene had already been transferred, etching the copper away, rinsing, and drying.

**Membrane Characterization.** SEM images were acquired with the JEOL 6320FV Field-Emission High-Resolution SEM at the MIT Center for Materials Science and Engineering. All images were obtained at an acceleration voltage of 5 kV in secondary electron imaging mode. Carbon tape was used to create a current path between the graphene on the GCM and the microscope

stage to reduce charging of the polycarbonate support material. The CVD graphene was characterized by Raman spectroscopy and scanning transmission electron microscopy with the results reported in ref 13.

**Gas Permeance Measurements.** Gas flow rates through the graphene composite membrane were measured using the apparatus sketched in the inset of Figure 2a. The membrane was sealed between an upstream pressure line and a downstream reservoir, both initially evacuated. During measurements, the upstream line was continuously supplied with a single gas species at an absolute pressure of 1 atm by a regulated gas cylinder. A pressure transducer was used to measure the rate of pressure rise in the downstream reservoir, resulting in time traces such as those presented in Figure 2b. The slope of the pressure-time line was used in an ideal gas law relation to determine the flow rate through the graphene membrane (see Supporting Information Section 2 for additional details on the measurement equipment and procedure).

**Conflict of Interest:** The authors declare no competing financial interest.

**Acknowledgment.** The authors thank J. Kong and Y. Song for helpful discussions and suggestions. Funding for this work was provided by the MIT Energy Initiative Seed Fund and the NSERC PGS program (to MSHB). This work made use of the MRSEC Shared Experimental Facilities at MIT, supported by the National Science Foundation under award number DMR-08-19762.

**Supporting Information Available:** Additional details on gas permeation models, gas flow rate measurement, and estimation of interlayer flux. This material is available free of charge via the Internet at <http://pubs.acs.org>.

## REFERENCES AND NOTES

- Baker, R. W. Future Directions of Membrane Gas Separation Technology. *Ind. Eng. Chem. Res.* **2002**, *41*, 1393–1411.
- Baker, R. W. Research Needs in the Membrane Separation Industry: Looking Back, Looking Forward. *J. Membr. Sci.* **2010**, *362*, 134–136.
- Adhikari, S.; Fernando, S. Hydrogen Membrane Separation Techniques. *Ind. Eng. Chem. Res.* **2006**, *45*, 875–881.
- D'Alessandro, D. M.; Smit, B.; Long, J. R. Carbon Dioxide Capture: Prospects for New Materials. *Angew. Chem., Int. Ed.* **2010**, *49*, 6058–6082.
- Baker, R. W.; Lokhandwala, K. Natural Gas Processing with Membranes: an Overview. *Ind. Eng. Chem. Res.* **2008**, *47*, 2109–2121.
- Jiang, D.-E.; Cooper, V. R.; Dai, S. Porous Graphene As the Ultimate Membrane for Gas Separation. *Nano Lett.* **2009**, *9*, 4019–4024.
- Schrier, J. Helium Separation Using Porous Graphene Membranes. *J. Phys. Chem. Lett.* **2010**, *1*, 2284–2287.
- Koenig, S. P.; Wang, L.; Pellegrino, J.; Bunch, J. S. Selective Molecular Sieving through Porous Graphene. *Nat. Nanotechnol.* **2012**, *7*, 728–732.
- Au, H. Molecular Dynamics Simulation of Nanoporous Graphene for Selective Gas Separation. MS Thesis, MIT: Cambridge, MA, 2012.
- Drahushuk, L. W.; Strano, M. S. Mechanisms of Gas Permeation through Single Layer Graphene Membranes. *Langmuir* **2012**, *28*, 16671–16678.
- Hauser, A. W.; Schwerdtfeger, P. Methane-Selective Nanoporous Graphene Membranes for Gas Purification. *Phys. Chem. Chem. Phys.* **2012**, *14*, 13292–13298.
- Bunch, J. S.; Verbridge, S. S.; Alden, J. S.; van der Zande, A. M.; Parpia, J. M.; Craighead, H. G.; McEuen, P. L. Impermeable Atomic Membranes from Graphene Sheets. *Nano Lett.* **2008**, *8*, 2458–2462.
- O'Hern, S. C.; Stewart, C. A.; Boutilier, M. S. H.; Idrobo, J.-C.; Bhaviripudi, S.; Das, S. K.; Kong, J.; Laoui, T.; Atieh, M.; Karnik, R. Selective Molecular Transport through Intrinsic Defects in a Single Layer of CVD Graphene. *ACS Nano* **2012**, *6*, 10130–10138.
- Nair, R. R.; Wu, H. A.; Jayaram, P. N.; Grigorieva, I. V.; Geim, A. K. Unimpeded Permeation of Water through Helium-Leak–Tight Graphene-Based Membranes. *Science* **2012**, *335*, 442–444.
- Kim, H. W.; Yoon, H. W.; Yoon, S.-M.; Yoo, B. M.; Ahn, B. K.; Cho, Y. H.; Shin, H. J.; Yang, H.; Paik, U.; Kwon, S.; Choi, J.-Y.; Park, H. B. Selective Gas Transport through Few-Layered Graphene and Graphene Oxide Membranes. *Science* **2013**, *342*, 91–95.
- Li, H.; Song, Z.; Zhang, X.; Huang, Y.; Li, S.; Mao, Y.; Ploehn, H.; Bao, Y.; Yu, M. Ultrathin, Molecular-Sieving Graphene Oxide Membranes for Selective Hydrogen Separation. *Science* **2013**, *342*, 95–98.
- Apel, P. Y.; Blonskaya, I.; Dmitriev, S.; Orelovitch, O.; Sartowska, B. Structure of Polycarbonate Track-Etch Membranes: Origin of the “Paradoxical” Pore Shape. *J. Membr. Sci.* **2006**, *282*, 393–400.
- Henis, J. M. S.; Tripodi, M. K. Composite Hollow Fiber Membranes for Gas Separation: the Resistance Model Approach. *J. Membr. Sci.* **1981**, *8*, 233–246.
- Breck, D. W. *Zeolite Molecular Sieves: Structure, Chemistry, and Use*; Wiley: New York, 1973; p 636.
- Yoon, T.; Mun, J. H.; Cho, B. J.; Kim, T.-S. Penetration and Lateral Diffusion Characteristics of Polycrystalline Graphene Barriers. *Nanoscale* **2014**, *6*, 151–156.